

Fragmentation Functions for Pions, Kaons, and Protons at Next-to-Leading Order

B.A. KNIEHL,¹ G. KRAMER,¹ B. PÖTTER²

¹ II. Institut für Theoretische Physik, Universität Hamburg,
Luruper Chaussee 149, 22761 Hamburg, Germany

² Max-Planck-Institut für Physik (Werner-Heisenberg-Institut),
Föhringer Ring 6, 80805 Munich, Germany

Abstract

We present new sets of fragmentation functions for charged pions, charged kaons, and protons, both at the leading and next-to-leading orders. They are fitted to the scaled-momentum distributions of these hadrons measured in e^+e^- annihilation on the Z -boson resonance at CERN LEP1 and SLAC SLC. These data partly come as light-, charm-, bottom-quark-enriched and gluon-jet samples, which allows us to treat all partons independently, after imposing the SU(2) flavour symmetry relations. In order to gain sensitivity to the scaling violation in fragmentation, we also include data from SLAC PEP, with center-of-mass energy $\sqrt{s} = 29$ GeV, in our fits. This allows us to also determine the strong-coupling constant, with a competitive error. LEP1 data on the longitudinal cross section as well as DESY DORIS and PETRA data at lower energies nicely agree with theoretical predictions based on our fragmentation functions.

PACS numbers: 13.65.+i, 13.85.Ni, 13.87.Fh

1 Introduction

The inclusive production of a single charged hadron, h , in the annihilation process

$$e^+e^- \rightarrow (\gamma, Z) \rightarrow h + X, \quad (1)$$

has been measured at many different e^+e^- colliders over a wide range of center-of-mass (CM) energies, \sqrt{s} , between 3 and 183 GeV [1,2]. Here, h may either refer to a specific hadron species, *e.g.*, pion, kaon, or proton, or to the sum over all charged-hadron species. A large amount of precise data has now become available from various experimental collaborations at CERN LEP1 and SLAC SLC, who started taking data several years ago. The process (1) is particularly suitable in order to study the fragmentation of quarks and gluons into hadrons. The information contained in fixed-target, hadron-collider, and ep -scattering data is less useful, since it is obscured by theoretical uncertainties from the parton distribution functions and the choice of factorization scales connected with the initial states.

The partonic cross sections pertinent to process (1) can be entirely calculated in perturbative QCD with no additional input, except for the strong-coupling constant α_s . They are known at next-to-leading order (NLO) [3] and even at next-to-next-to-leading order (NNLO) [4]. The subsequent transition of the partons into hadrons takes place at an energy scale of the order of 1 GeV and can, therefore, not be treated in perturbation theory. Instead, the hadronization of the partons is described by fragmentation functions (FFs), $D_a^h(x, Q^2)$. Their values correspond to the probability that the parton a , which is produced at short distance, of order $1/Q$, fragments into the hadron h carrying the fraction x of the momentum of a . In the case of process (1), Q^2 is typically of order s . Given their x dependence at some scale Q_0^2 , the evolution of the FFs with Q^2 may be computed perturbatively. At present, the evolution equations are only known through NLO. Consistency requires that we do not include the NNLO corrections to the partonic cross sections [4] in our analysis of process (1) via unpolarized photons and Z bosons.

The theoretical analysis of the fragmentation process in e^+e^- annihilation is of interest for several reasons. First, it allows us to test QCD quantitatively within one experiment observing hadrons at different values of \sqrt{s} and to determine the strong-coupling constant, $\alpha_s(Q)$, to be compared with determinations from other observables and/or processes. Second, since according to the factorization theorem the FFs are independent of the process in which they have been determined, they can be used for quantitative predictions of inclusive single hadron cross sections in other processes, like $p\bar{p}$, ep , γp , and $\gamma\gamma$ scattering. Third, the exact knowledge of the FFs, in particular for identified hadrons, may help to elucidate the fundamental features of hadronization and to constrain models used for the calculation of complete final states in various high-energy reactions.

After the pioneering leading-order (LO) analyses of pion, kaon [5,6], and charmed-meson [7] FFs in the late 70s, there had long been no progress on the theoretical side of this field. In the mid 90's, NLO FF sets for π^0 [8], π^\pm , K^\pm , and η mesons [9] have been constructed through fits to data of e^+e^- annihilation, mostly generated with Monte Carlo event generators.

In 1994/95, two of us, together with Binnewies, determined the FFs of quarks and gluons into π^\pm and K^\pm mesons at LO and NLO from genuine experimental data, adopting two different strategies [10,11]. In the first analysis [10], we included in the fit only the data on π^\pm and K^\pm production taken by the TPC/Two-Gamma Collaboration [12] at SLAC PEP, with energy $\sqrt{s} = 29$ GeV. These data combine small statistical errors with fine binning in x and are thus more constraining than data collected by other experiments in the energy range from 5.2 GeV to 44 GeV. Charged-pion and -kaon data at other energies were only used for cross checks. Furthermore, theoretical predictions obtained using these FFs were compared with data on the inclusive production of unidentified charged hadrons taken at the PEP, DESY PETRA, and KEK TRISTAN colliders making an assumption on the p/\bar{p} contribution based on information extracted from the TPC data [12]. In 1994, when the first analysis [10] was performed, data with identified quark flavours did not exist. Therefore, we had to make the assumption that the s , c , and b (d , c , and b) quarks fragment into π^\pm (K^\pm) mesons in the same way.

In our second analysis [11], we could remove this assumption because new data on charged-hadron production with partial flavour separation had been released by the ALEPH Collaboration [13] at LEP1 (see also Refs. [2,14,15]). Apart from the usual data sample without flavour separation, they also presented light- and b -quark-enriched samples. Here and in the following, we consider u , d , and s quarks as light. In addition, we included in our fits accurate π^\pm and K^\pm data from ALEPH [16] and information on tagged three-jet events from OPAL [17] at LEP1, which constrained the gluon FFs. In order to describe the production of charged hadrons in terms of the π^\pm and K^\pm FFs, we needed some information on the fragmentation of quarks and gluons into protons and antiprotons. To that end, we introduced a function $f(x)$ which parameterizes the ratio of the p/\bar{p} and π^\pm production cross sections as measured by ALEPH [16].

It is clear that this analysis [11] suffered from the lack of specific data on the fragmentation of tagged quarks and gluons to π^\pm , K^\pm , and p/\bar{p} hadrons, rather than just to charged hadrons of unidentified species. This lack has been remedied in 1998 by the advent of new data from DELPHI [18] at LEP1 and SLD [19] at SLC. Besides other things, SLD [19] measured the differential production cross section, as a function of the scaled momentum $x = 2p/\sqrt{s}$, for the identified hadron species π^\pm , K^\pm , and p/\bar{p} in Z -boson decays to light, c , and b quarks and in such decays without flavour separation. Similarly, DELPHI [18] presented π^\pm , K^\pm , and p/\bar{p} production data, covering the full momentum range up to 45.6 GeV, discriminating between $Z \rightarrow u\bar{u}, d\bar{d}, s\bar{s}$, $Z \rightarrow b\bar{b}$, and $Z \rightarrow q\bar{q}$ events. There is also new specific information that allows us to better control the gluon FF. In fact, new gluon-tagged three-jet data of inclusive charged-hadron production was released by ALEPH [20] and OPAL [21]. In the OPAL [21] analysis, the gluon jets were identified using the method proposed by Gary [22]. This method is based on rare events of the type $e^+e^- \rightarrow q\bar{q}g_{\text{incl}}$ in which the q - and \bar{q} -quark jets appear in the same hemisphere of a multihadronic e^+e^- annihilation event. The object g_{incl} , which is taken to be the gluon jet, is defined by all hadrons observed in the hemisphere opposite to that containing the q - and \bar{q} -quark jets. This method allows for the extraction of the gluon FF with as little theoretical bias as possible. It is supposed to be superior to the earlier OPAL [17] mea-

surement of the gluon FF based on a jet-finding algorithm to define the gluon jets, which entered the BKK analysis [11]. The new OPAL [21] data set comprises more points than the previous one [17], and the energy of the gluon jets is now well defined, with a mean value of $E_{\text{jet}} = 40.1$ GeV.

It is the purpose of this work to make full use of all the recent data from ALEPH [20], DELPHI [18], OPAL [21], and SLD [19] in order to construct new sets of LO and NLO FFs without imposing relations between the FFs of different flavours, except that we identify the FFs of u and d quarks into π^\pm mesons and those of u and s quarks into K^\pm mesons, as in Refs. [10,11]. In the case of protons and antiprotons, we fix the d -quark FFs to be half of the u -quark FFs. For completeness, we also include in our fits the older π^\pm , K^\pm , and p/\bar{p} production data without flavour separation from ALEPH [16], which also entered the BKK analysis [11]. In order to be sensitive to the running of α_s , *i.e.*, to be able to fit the asymptotic scale parameter, $\Lambda_{\overline{\text{MS}}}^{(5)}$, we also include the TPC data [12], as in Refs. [10,11]. There is also precise data on charged-hadron production with flavour separation from ALEPH [14,15], who provided light-, c -, and b -quark-enriched samples, and from OPAL [23], who provided light- and b -quark-enriched samples. To be on the conservative side, we exclude this data from our fits because the contribution due to charged hadrons other than π^\pm , K^\pm , and p/\bar{p} is unknown and may be comparable or larger than the experimental errors. In fact, it turns out that this data yields rather sizeable χ^2 values relative to the theoretical predictions obtained from our FFs. We also test our FFs against data from e^+e^- colliders with lower CM energies, namely, from DESY DORIS [24,25] and PETRA [26,27]. Furthermore, we study the longitudinal cross section for the production of charged hadrons on the Z -boson resonance and compare the results with data from ALEPH [14], DELPHI [28], and OPAL [29].

This work is organized as follows. In Section 2, we summarize the data included in our fits, outline the theoretical framework, describe our fitting procedure, present our FFs, and discuss their goodness. Furthermore, we check our FFs against e^+e^- data which are not included in our fits. In Section 3, we investigate for charged-hadron production how well our FFs satisfy the momentum sum rule, which we did not impose on our fits. Furthermore, we examine to what extent our FFs also account for the longitudinal cross section of charged-hadron production on the Z -boson resonance, and how our NLO gluon FF compares with the one of the BKK set [11] and with the one recently measured by DELPHI [30]. Our conclusions are summarized in Section 4.

2 Analysis and Results

We start by summarizing the experimental data which are used for our fits or for comparisons. We include in our fits the π^\pm , K^\pm , and p/\bar{p} data with flavour separation from DELPHI [18] and SLD [19] and those without flavour separation from ALEPH [16], DELPHI [18], SLD [19], and TPC [12]. Furthermore, we use the charged-hadron data with flavour separation from DELPHI [18] and those without flavour separation from SLD [19]. In order to constrain the gluon FFs, we employ the gluon-tagged three-jet data without

Table 1: CM energies, types of data, and χ^2_{DF} values obtained at LO and NLO for various data samples. Samples not used in the fits are marked by asterisks.

\sqrt{s} [GeV]	Data type	χ^2_{DF} in NLO			χ^2_{DF} in LO		
29.0	σ^π (all)	0.64 [12]			0.71 [12]		
	σ^K (all)	1.86 [12]			1.40 [12]		
	σ^p (all)	0.79 [12]			0.70 [12]		
91.2	σ^h (all)	1.28 [18]	48.1 [15]*	14.4 [23]*	1.40 [18]	53.1 [15]*	15.8 [23]*
		1.32 [19]			1.44 [19]		
	σ^h (uds)	0.20 [18]	89.4 [14]*	5.10 [23]*	0.20 [18]	92.1 [14]*	4.60 [23]*
	σ^h (c)		80.1 [14]*	0.51 [23]*		58.9 [14]*	0.45 [23]*
	σ^h (b)	0.43 [18]	221 [14]*	6.63 [23]*	0.41 [18]	220 [14]*	6.33 [23]*
	σ^π (all)	1.28 [16]	0.58 [18]	3.09 [19]	1.65 [16]	0.60 [18]	3.13 [19]
	σ^π (uds)		0.72 [18]	1.87 [19]		0.73 [18]	2.17 [19]
	σ^π (c)			1.36 [19]			1.16 [19]
	σ^π (b)		0.57 [18]	1.00 [19]		0.58 [18]	0.99 [19]
	σ^K (all)	0.30 [16]	0.86 [18]	0.44 [19]	0.32 [16]	0.79 [18]	0.45 [19]
	σ^K (uds)		0.53 [18]	0.65 [19]		0.60 [18]	0.64 [19]
	σ^K (c)			2.11 [19]			1.90 [19]
	σ^K (b)		0.14 [18]	1.21 [19]		0.14 [18]	1.23 [19]
	σ^p (all)	0.93 [16]	0.09 [18]	0.79 [19]	0.80 [16]	0.06 [18]	0.70 [19]
	σ^p (uds)		0.11 [18]	1.29 [19]		0.14 [18]	1.28 [19]
	σ^p (c)			0.92 [19]			0.89 [19]
	σ^p (b)		0.56 [18]	0.97 [19]		0.62 [18]	0.89 [19]
E_{jet} [GeV]							
26.2	D_g^h	1.19 [20]			1.18 [20]		
40.1	D_g^h	1.03 [21]			0.90 [21]		

hadron identification from ALEPH [20] and OPAL [21]. The charged-hadron data without and with flavour separation from ALEPH [14,15] and OPAL [23] are only used for comparison. All these data sets are summarized in Table 1.

The key observable of the experimental analyses and our study is the scaled-momentum distribution normalized to the total hadronic cross section, $(1/\sigma_{\text{tot}})d\sigma^h/dx$. In general, the scaled momentum is defined as $x = 2p/\sqrt{s}$, where p is the three-momentum of the observed hadron in the CM frame. In three-jet events, one often defines $x = p/E_{\text{jet}}$, where E_{jet} is the gluon-jet energy in the CM frame. By charge-conjugation invariance, the e^+e^- cross sections for π^+ , K^+ , and p production should be the same as those for π^- , K^- , and \bar{p} production, respectively. Therefore, one usually sums over both charges, which is also true for the production of unidentified charged hadrons. In turn, also our FFs refer to the sums of particles and antiparticles.

The LO and NLO formalisms for extracting FFs from e^+e^- data were comprehensively described in Refs. [10,11] and will, therefore, not be reviewed here. The NLO formula for $d\sigma^h/dx$ was originally obtained in Ref. [3] and is given in Eq. (3) of Ref. [11]. Deviating

from Refs. [10,11], we calculate σ_{tot} including QCD corrections up to $\mathcal{O}(\alpha_s^2)$. We work in the $\overline{\text{MS}}$ renormalization and factorization scheme and choose the renormalization scale μ and the factorization scale M_f to be $\mu = M_f = \sqrt{s}$, except for gluon-tagged three-jet events, where we put $\mu = M_f = 2E_{\text{jet}}$. For the actual fitting procedure, we use x bins in the interval $0.1 \leq x \leq 1$ and integrate the theoretical functions over the bins width as is done in the experimental analyses. The restriction at small x is introduced to exclude events in the nonperturbative region, where mass effects and nonperturbative intrinsic-transverse-momentum (k_T) effects are important and the underlying formalism is insufficient. We parameterize the x dependence of the FFs at the starting scale Q_0 as

$$D_a^h(x, Q_0^2) = Nx^\alpha(1-x)^\beta. \quad (2)$$

As in Ref. [11], we use $Q_0 = \sqrt{2}$ GeV for $a = u, d, s, g$, $Q_0 = m(\eta_c) = 2.9788$ GeV for $a = c$, and $Q_0 = m(\Upsilon) = 9.46037$ GeV for $a = b$. We impose the conditions

$$\begin{aligned} D_u^{\pi^\pm}(x, Q_0^2) &= D_d^{\pi^\pm}(x, Q_0^2), \\ D_u^{K^\pm}(x, Q_0^2) &= D_s^{K^\pm}(x, Q_0^2), \\ D_u^{p/\bar{p}}(x, Q_0^2) &= 2D_d^{p/\bar{p}}(x, Q_0^2), \end{aligned} \quad (3)$$

which are suggested by the valence quark composition of the respective hadrons. Equations (3) are preserved by the Q^2 evolution. The constraint on the K^\pm FFs should be slightly violated by the mass difference between the u and s quarks [5]. In fact, the $s \rightarrow K^-$ transition should happen more frequently than the $\bar{u} \rightarrow K^-$ one because less energy is needed for the creation of a $u\bar{u}$ pair from the vacuum than for a $s\bar{s}$ pair. However, we shall neglect this subtlety in our analysis because the presently available experimental information is not rich enough to resolve such minor differences. For all the other FFs, we treat N , α , and β as independent fit parameters. In addition, we take the asymptotic scale parameter $\Lambda_{\overline{\text{MS}}}^{(5)}$, appropriate for five quark flavours, as a free parameter. Thus, we have a total of 46 independent fit parameters. The quality of the fit is measured in terms of the χ^2 value per degree of freedom, χ_{DF}^2 , for all selected data points. Using a multi-dimensional minimization algorithm [31], we search this 46-dimensional parameter space for the point at which the deviation of the theoretical prediction from the data becomes minimal.

The χ_{DF}^2 values achieved for the different data sets used in our LO and NLO fits may be seen from Table 1. Most of the χ_{DF}^2 values lie around 1 or below, indicating that the fitted FFs describe all data sets within their respective errors. In general, the χ_{DF}^2 values come out in favour of the DELPHI [18] data. The overall goodness of the NLO (LO) fit is given by $\chi_{\text{DF}}^2 = 0.98$ (0.97). In Table 1, we have also specified the χ_{DF}^2 values for those data sets which we have discussed above, but not included in the fits [14,15,23]. Some of these sets come out with much higher χ_{DF}^2 values than those included in the fits, which will be discussed in detail later. The values of the parameters N , α , and β in Eq. (2) resulting from the LO and NLO fits are collected in Table 2. They refer to the fragmentation of the partons $a = u, d, s, c, b, g$ into the hadrons $h = \pi^\pm, K^\pm, p/\bar{p}$, where the sum over particles and antiparticles is implied.

Table 2: Values of N , α , and β in Eq. (2) resulting from the NLO fit. The numbers given in parentheses refer to the LO fit.

Hadron	Flavour	N	α	β
π^\pm	$u = d$	0.448 (0.546)	-1.48 (-1.47)	0.913 (1.02)
	s	16.6 (22.3)	0.133 (0.127)	5.90 (6.14)
	c	6.17 (8.76)	-0.536 (-0.386)	5.60 (5.62)
	b	0.259 (0.311)	-1.99 (-1.93)	3.53 (3.47)
	g	3.73 (6.05)	-0.742 (-0.714)	2.33 (2.92)
K^\pm	$u = s$	0.178 (0.259)	-0.537 (-0.619)	0.759 (0.859)
	d	4.96 (5.38)	0.0556 (-0.00321)	2.80 (3.08)
	c	4.26 (5.18)	-0.241 (-0.178)	4.21 (4.30)
	b	1.32 (1.57)	-0.884 (-0.841)	6.15 (6.01)
	g	0.231 (0.0286)	-1.36 (-2.94)	1.80 (2.73)
p/\bar{p}	$u = 2d$	1.26 (0.402)	0.0712 (-0.860)	4.13 (2.80)
	s	4.01 (4.08)	0.173 (-0.0974)	5.21 (4.99)
	c	0.0825 (0.111)	-1.61 (-1.54)	2.01 (2.21)
	b	24.3 (40.1)	0.579 (0.742)	12.1 (12.4)
	g	1.56 (0.740)	0.0157 (-0.770)	3.58 (7.69)

Since we included in our fits high-quality data from two very different energies, namely 29 and 91.2 GeV, we are sensitive to the running of $\alpha_s(\mu)$ and are, therefore, able to extract values of $\Lambda_{\overline{\text{MS}}}^{(5)}$. We obtain $\Lambda_{\overline{\text{MS}}}^{(5)} = 213_{-73}^{+75}$ MeV at NLO and $\Lambda_{\overline{\text{MS}}}^{(5)} = 88_{-31}^{+34}$ MeV at LO. This corresponds to $\alpha_s(M_Z) = 0.1170_{-0.007}^{+0.005}$ at NLO and $\alpha_s(M_Z) = 0.1181_{-0.007}^{+0.006}$ at LO. Here, the errors are determined by varying $\Lambda_{\overline{\text{MS}}}^{(5)}$ in such a way that the total χ_{DF}^2 is increased by one unit if all the other fit parameters are kept fixed. They do not include theoretical errors, which may be estimated through variations of the overall scale $\mu = M_f$. Our NLO values for $\Lambda_{\overline{\text{MS}}}^{(5)}$ and $\alpha_s(M_Z)$ perfectly agree with those presently quoted by the Particle Data Group as world averages, $\Lambda_{\overline{\text{MS}}}^{(5)} = 212_{-23}^{+25}$ MeV and $\alpha_s(M_Z) = 0.1185 \pm 0.002$, respectively [32]. We note, however, that in Ref. [32] the value of $\Lambda_{\overline{\text{MS}}}^{(5)}$ is obtained from $\alpha_s(M_Z)$ through the next-to-next-to-leading-order formula for $\alpha_s(\mu)$, while we use the LO and NLO formulas, depending on the order of our analysis, as is required by consistency. Since the errors on $\alpha_s(\mu)$ and $\Lambda_{\overline{\text{MS}}}^{(5)}$ quoted in Ref. [32] result from an average of different kinds of measurements, they are considerably smaller than those obtained here from a single type of experiment. In this context, we remark that, throughout our analysis, we assume nonperturbative power corrections proportional to $1/Q$ to be negligible in the energy range relevant for our fits.

The goodness of our LO and NLO fits to the ALEPH [16,20], DELPHI [18], OPAL [21], and SLD [19] data may be judged from Figs. 1–5. In Figs. 1–4, we study the cross

section $(1/\sigma_{\text{tot}})d\sigma^h/dx$ of charged-hadron, π^\pm , K^\pm , and p/\bar{p} production, respectively, at $\sqrt{s} = 91.2$ GeV as a function of x . In Fig. 1, the contributions from all quark flavours and the gluon are included, while Figs. 2–4 refer to the fragmentation of light, c , and b quarks, respectively. As in the experimental analyses [14,15,18,19,23], we have to arrange for the latter three contributions to add up to the first one. Therefore, we distribute the gluon contribution among the various quark contributions according to their electroweak coupling strengths to the neutral current. In this way, the gluon radiation off a quark line of a given flavour is accounted towards the contribution of this quark flavour. The theoretical results are compared with the respective data from ALEPH [16] in Fig. 1, with that from DELPHI [18] in Figs. 1, 2, and 4, and with that from SLD [19] in Figs. 1–4. We observe that, in all cases, the various data are mutually consistent with each other and are nicely described by the LO and NLO fits, which is also reflected in the relatively small χ^2_{DF} values given in Table 1. The LO and NLO fits are almost indistinguishable in those regions of x , where the data have small errors. For large x , where the statistical errors are large, the LO and NLO results sometimes moderately deviate from each other.

In Fig. 5, we compare the ALEPH [20] and OPAL [21] measurements of the gluon FF in charged-hadron production, which comprises five and twelve data points, respectively, with our LO and NLO fit results. The scale choice is $\mu = M_f = 2E_{\text{jet}}$, with $E_{\text{jet}} = 26.2$ [20] and 40.1 GeV [21], respectively. The data are nicely fitted, with χ^2_{DF} values of order unity, as may be seen from Table 1. By the same token, this implies that the data are mutually consistent.

As may be seen from Table 1, the ALEPH [14,15] and OPAL [23] data on charged-hadron production with and without flavour separation, which are excluded from our fits, lead to rather sizeable χ^2_{DF} values relative to the theoretical predictions based on our FFs. They are obviously inconsistent with the DELPHI [18] and SLD [19] data included in our fits. In particular, the flavour-enriched charged-hadron samples from ALEPH [14] give χ^2_{DF} values of order 100. The comparison of these ALEPH [14,15] and OPAL [23] data with our LO and NLO predictions is also illustrated in Fig. 6. We should point out that the ALEPH [14,15,16] data possess the following property. The sum of the three flavour-tagged cross sections of charged-hadron production [14], which agrees with the charged-hadron cross section without flavour separation quoted in Ref. [15], appreciably overshoots the sum of the π^\pm , K^\pm , and p/\bar{p} cross sections without flavour separation, which stem from an independent measurement [16]. The latter three data sets [16] are included in our fits and lead to quite acceptable χ^2_{DF} values, as may be seen from Table 1. We remark that the charged-hadron data with flavour separation from ALEPH [14] served as one of the main inputs for the BKK analysis [11]. We attribute this difference to the contribution from charged hadrons other than π^\pm , K^\pm , and p/\bar{p} hadrons, which may be comparable or larger than the relatively small errors on the charged-hadron data [14,15]. We assume that this interpretation is also valid for the OPAL data [23]. On the contrary, the DELPHI [18] and SLD [19] analyses are based on the assumption that the sum of the π^\pm , K^\pm , and p/\bar{p} data exhaust the full charged-hadron data. In want of a separate measurement of the excess in cross section due to high-mass charged hadrons, we decided to proceed as in Refs. [18,19].

Table 3: CM energies, types of data, and χ^2_{DF} values obtained at LO and NLO for various pre-LEP/SLC data samples not included in our fits.

\sqrt{s} [GeV]	Data type	χ^2_{DF} in NLO	χ^2_{DF} in LO
5.4	σ^π (all)	3.10 [24]	3.02 [24]
	σ^K (all)	1.80 [24]	2.33 [24]
9.98	σ^π (all)	3.27 [25]	2.78 [25]
	σ^K (all)	3.21 [25]	2.81 [25]
22.0	σ^p (all)	1.29 [26]	1.50 [26]
34.0	σ^π (all)	0.80 [27]	0.88 [27]
	σ^K (all)	0.31 [27]	0.37 [27]
	σ^p (all)	0.58 [27]	0.46 [27]

We now report on comparisons with pre-LEP/SLC data on π^\pm , K^\pm , and $p\bar{p}$ production which we did not include in our fits. Specifically, we consider the π^\pm and K^\pm data from DASP [24] ($\sqrt{s} = 5.2$ GeV) and ARGUS [25] ($\sqrt{s} = 9.98$ GeV) at DESY DORIS and from TASSO [27] ($\sqrt{s} = 34$ GeV) at PETRA, and the p/\bar{p} data taken by TASSO at $\sqrt{s} = 22$ [26] and 34 GeV [27]. There is no separation into flavour-enriched or three-jet samples for this data. The resulting χ^2_{DF} values are summarized in Table 3. As in the fits, they are evaluated only taking into account the data points with $x \geq 0.1$. The comparison of the π^\pm , K^\pm , and p/\bar{p} data with our LO and NLO predictions is visualized in Figs. 7–9, respectively. For reference, also the corresponding TPC [12] and SLC [19] data are included in these comparisons. From Table 3 and Figs. 7–9, we learn that the DASP [24], ARGUS [25], and TASSO [26,27] data agree quite well with our LO and NLO predictions. This concludes the description of our fitting procedure and of the quality of the fits.

3 Applications

We now investigate if our FFs satisfy the momentum sum rules. Since a given parton a fragments with 100% likelihood into some hadron h and momentum is conserved during the fragmentation process, we have

$$\int_0^1 dx x D_a^h(x, Q^2) = 1, \quad (4)$$

for any value of Q^2 . As is well established experimentally, even for the flavour-enriched data samples [19,18], the sum of the π^\pm , K^\pm , and p/\bar{p} production cross sections agrees, to good approximation, with the one of charged-hadron production. Thus, insertion of our π^\pm , K^\pm , and p/\bar{p} FFs in Eq. (4) exhausts the charged-hadron contribution. As for the neutral-hadron FFs, which also enter Eq. (4), we make the following assumptions which

are suggested by SU(2) flavour symmetry. As in Ref. [11], we approximate

$$\begin{aligned} D_a^{\pi^0}(x, Q^2) &= \frac{1}{2} D_a^{\pi^\pm}(x, Q^2), \\ D_{u,d,s,c,b,g}^{K^0/\bar{K}^0}(x, Q^2) &= D_{d,u,s,c,b,g}^{K^\pm}(x, Q^2). \end{aligned} \quad (5)$$

Furthermore, we assume that

$$\begin{aligned} D_u^{n/\bar{n}}(x, Q^2) &= \frac{1}{2} D_u^{p/\bar{p}}(x, Q^2), \\ D_d^{n/\bar{n}}(x, Q^2) &= 2 D_d^{p/\bar{p}}(x, Q^2), \\ D_{s,c,b,g}^{n/\bar{n}}(x, Q^2) &= D_{s,c,b,g}^{p/\bar{p}}(x, Q^2). \end{aligned} \quad (6)$$

Here, $D_a^{\pi^\pm}(x, Q^2)$, $D_a^{K^0/\bar{K}^0}(x, Q^2)$, *etc.* refer to the sums of the FFs for the individual hadron species. Equations (5) are supported by e^+e^- data of pion [2,33] and kaon [34] production, except for very small x . To be on the conservative side, we take the lower limit of integration in Eq. (4) to be 0.05 rather than 0, so that the FF parameterizations are not used too far outside the x range which was selected for the fits. This particular choice may be motivated by observing that the π^\pm , K^\pm , and p/\bar{p} data sets in Figs. 7–9 are well described by the theoretical predictions down to x values of order 0.05. Since we leave out the x range below 0.05, our results for the left-hand side of Eq. (4) are expected to be somewhat below unity. A more sophisticated approach [35] would be to improve the description of the low- x region by modifying our ansatz for the FFs according to the so-called modified leading logarithmic approximation (MLLA) [36].

In Table 4, we list the results obtained with our LO and NLO FFs for $Q = \sqrt{2}$, 4, 10, 91, and 200 GeV. The accuracy of our results is limited by the uncertainties in our assumptions (5) and (6), in particular for the lower values of Q . In the case of the d quark, we find values slightly larger than unity at small values of Q , both in LO and NLO. On the other hand, the s -quark values are considerably smaller than unity, in particular in NLO. The gluon FF gives values appreciably larger than unity at small values of Q , both in LO and NLO. We believe that the imbalance between the d - and s -quark results is due to our limited knowledge of the relative magnitude of the valence- and light-sea-quark contents of the π^\pm , K^\pm , and p/\bar{p} hadrons. Since the u , d , and s quarks are always combined in the available data, there are no individual constraints on their FFs. In order to trace the source of this imbalance, let us consider the π^\pm and K^\pm contributions to the left-hand side of Eq. (4) at $Q_0 = \sqrt{2}$ GeV for $a = u, d, s$. In the case of π^\pm , we have

$$\begin{aligned} \int_{0.05}^1 dx x D_{u,d}^{\pi^\pm}(x, Q_0^2) &= 0.41, \\ \int_{0.05}^1 dx x D_s^{\pi^\pm}(x, Q_0^2) &= 0.23, \end{aligned} \quad (7)$$

which nicely exhibits the valence-like character of the u and d quarks in contrast to the sea-like character of the s quark. In the case of K^\pm , however, we find

$$\int_{0.05}^1 dx x D_{u,s}^{K^\pm}(x, Q_0^2) = 0.19,$$

Table 4: Left-hand side of Eq. (4) at NLO for $a = u, d, s, c, b, g$ and $Q = \sqrt{2}, 4, 10, 91, 200$ GeV. We sum over $h = \pi^\pm, \pi^0, K^\pm, K^0, \bar{K}^0, p, \bar{p}, n, \bar{n}$ and integrate over $0.05 \leq x \leq 1$. The numbers given in parentheses are evaluated with our LO set.

a	Q [GeV]				
	$\sqrt{2}$	4	10	91	200
u	0.96 (1.13)	0.96 (1.06)	0.92 (1.00)	0.82 (0.87)	0.78 (0.83)
d	1.05 (1.14)	1.05 (1.07)	1.00 (1.01)	0.89 (0.88)	0.85 (0.84)
s	0.60 (0.82)	0.68 (0.82)	0.67 (0.78)	0.62 (0.69)	0.60 (0.67)
c	–	0.91 (0.97)	0.88 (0.93)	0.78 (0.81)	0.75 (0.78)
b	–	–	0.73 (0.80)	0.65 (0.69)	0.62 (0.66)
g	1.33 (1.85)	1.15 (1.32)	1.00 (1.10)	0.73 (0.74)	0.67 (0.67)

$$\int_{0.05}^1 dx x D_d^{K^\pm}(x, Q_0^2) = 0.25, \quad (8)$$

which shows that the d quark does not behave sea-like, contrary to expectations. We have thus identified the non-sea-like behaviour of the d quark in the K^\pm mesons as the source of the violation of the sum rule in Table 4.

The analysis of the the longitudinal cross section offers a unique opportunity to test the gluon FF. The total cross section of inclusive hadron (h) production, which we have considered so far, may be decomposed into a transverse (T) and a longitudinal (L) component, $d\sigma^h/dx = d\sigma_T^h/dx + d\sigma_L^h/dx$, as indicated in Eq. (3) of Ref. [11]. As is well known, at $\mathcal{O}(\alpha_s^0)$, only transversely polarized photons and Z bosons contribute to the cross section. The longitudinal cross section $d\sigma_L^h/dx$ first appears at $\mathcal{O}(\alpha_s)$. Thus, one needs to know it through $\mathcal{O}(\alpha_s^2)$ in order to test the gluon FF in NLO. The $\mathcal{O}(\alpha_s^2)$ correction to $d\sigma_L^h/dx$ has been calculated in Refs. [4,37]. In the case of inclusive hadron production, $d\sigma_L^h/dx$ is given by a convolution of the longitudinal partonic cross sections with the corresponding FFs and has the following form [37]:

$$\begin{aligned} \frac{1}{\sigma_{\text{tot}}} \frac{d\sigma_L^h}{dx} = \int_x^1 \frac{dz}{z} \left\{ \left(\sum_{i=1}^{N_F} Q_{q_i}(s) \right) \left[\frac{1}{N_F} D_\Sigma^h \left(\frac{x}{z}, M_f^2 \right) \frac{1}{\sigma_{\text{tot}}} \frac{d\sigma_{L,q}^\Sigma}{dz} + D_g^h \left(\frac{x}{z}, M_f^2 \right) \frac{1}{\sigma_{\text{tot}}} \frac{d\sigma_{L,g}}{dz} \right] \right. \\ + \sum_{i=1}^{N_F} Q_{q_i}(s) D_{(+),i}^h \left(\frac{x}{z}, M_f^2 \right) \frac{1}{\sigma_{\text{tot}}} \frac{d\sigma_{L,q}^{\text{NS}}}{dz} \\ \left. + \sum_{i=1}^{N_F} Q_{q_i}^F(s) \left[D_{(+),i}^h \left(\frac{x}{z}, M_f^2 \right) + \frac{1}{N_F} D_\Sigma^h \left(\frac{x}{z}, M_f^2 \right) \right] \frac{1}{\sigma_{\text{tot}}} \frac{d\sigma_{L,q}^F}{dz} \right\}. \quad (9) \end{aligned}$$

Here, $N_C = 3$ and $N_F = 5$ denote the numbers of colours and active quark flavours, respectively, and $Q_{q_i}(s)$ and $Q_{q_i}^F(s)$ represent the effective electroweak couplings of the

quarks to the photon and Z boson. The latter are defined as

$$\begin{aligned}
Q_{q_i}(s) &= e_e^2 e_{q_i}^2 + 2e_e v_e e_{q_i} v_{q_i} \frac{s(s - M_Z^2)}{(s - M_Z^2)^2 + M_Z^2 \Gamma_Z^2} \\
&\quad + (v_e^2 + a_e^2) (v_{q_i}^2 + a_{q_i}^2) \frac{s^2}{(s - M_Z^2)^2 + M_Z^2 \Gamma_Z^2}, \\
Q_{q_i}^F(s) &= (v_{q_i}^2 + a_{q_i}^2) a_{q_i} \left(\sum_{j=1}^{N_F} a_{q_j} \right) \frac{s(s - M_Z^2)}{(s - M_Z^2)^2 + M_Z^2 \Gamma_Z^2},
\end{aligned} \tag{10}$$

where M_Z and Γ_Z are the mass and width of the Z boson, respectively, e_f is the electric charge of the fermion f in units of the positron charge, $v_f = (T_{3,f} - 2e_f \sin^2 \theta_w) / (2 \sin \theta_w \cos \theta_w)$ and $a_f = T_{3,f} / (2 \sin \theta_w \cos \theta_w)$ are its vector and axial-vector couplings to the Z boson, respectively, $T_{3,f}$ is the third component of isospin of its left-handed component, and θ_w is the electroweak mixing angle. In the limit $s \ll M_Z^2$, only the QED contribution survives, and we have $Q_{q_i} \rightarrow e_e^2 e_{q_i}^2$ and $Q_{q_i}^F \rightarrow 0$. The labels Σ and NS in Eq. (9) indicate the flavour singlet and flavour non-singlet contributions, which are related to the FF combinations

$$\begin{aligned}
D_{\Sigma}^h(x, M_f^2) &= \sum_{i=1}^{N_F} [D_{q_i}^h(x, M_f^2) + D_{\bar{q}_i}^h(x, M_f^2)], \\
D_{(+),i}^h(x, M_f^2) &= D_{q_i}^h(x, M_f^2) + D_{\bar{q}_i}^h(x, M_f^2) - \frac{1}{N_F} D_{\Sigma}^h(x, M_f^2).
\end{aligned} \tag{11}$$

The contributions proportional to the colour factor $C_F T_R = 4/8$ are labeled F , which is to suggest that they vanish in QED due to Furry's theorem. They only arise from Z -boson exchange, provided one does not sum over all quark flavours belonging to one fermion generation. Furthermore, they are devoid of collinear singularities, so that mass factorization is not needed. We neglect these contributions, since they amount to less than 1% over the whole x range [37]. The partonic cross sections $d\sigma_{L,q}^{\Sigma}/dz$, $d\sigma_{L,g}^{\Sigma}/dz$, and $d\sigma_{L,q}^{\text{NS}}/dz$ through $\mathcal{O}(\alpha_s^2)$ may be found in Refs. [4,37].

ALEPH [14], DELPHI [28], and OPAL [29] have measured $d\sigma_L^h/dx$ for charged-hadron production as a function of x without quark flavour separation. In addition, DELPHI [28] has also presented light- and b -quark-enriched samples. In Fig. 10, these data are compared with the LO and NLO evaluations of Eq. (9) with our FFs. As in our fits to data of $d\sigma^h/dx$, we choose the scales to be equal to the CM energy $\sqrt{s} = 91.2$ GeV, where the data have been taken. Although only data with $x \geq 0.1$ has been included in our fits, $d\sigma_L^h/dx$ is also well described down to $x = 0.01$. The χ_{DF}^2 values, evaluated from the data points with $x \geq 0.1$, are collected in Table 5. The χ_{DF}^2 values for the LO predictions are in average more than a factor of two larger than those for the NLO predictions. This is not surprising, since it was already found in Ref. [11] that the LO result falls short of the data by a factor of two. At that time, the common scale had to be reduced to 20 GeV in order to obtain agreement. We observe from Fig. 10 and Table 5 that this is no longer necessary for the NLO results. Obviously, the $\mathcal{O}(\alpha_s^2)$ corrections [4,37] are sufficient to

Table 5: CM energies, types of data, and χ^2_{DF} values obtained at LO and NLO for the longitudinal cross section.

\sqrt{s} [GeV]	Data type	χ^2_{DF} in NLO			χ^2_{DF} in LO		
91.2	σ_L^h (all)	1.36 [14]	1.74 [28]	0.49 [29]	11.0 [14]	1.27 [28]	7.94 [29]
	σ_L^h (uds)		7.98 [28]			1.05 [28]	
	σ_L^h (b)		0.51 [28]			0.80 [28]	

produce a K factor that brings our predictions into good agreement with the data. Good agreement between the NLO prediction of $d\sigma_L^h/dx$ and the ALEPH [14] and OPAL [29] data was already found by Rijken and van Neerven [4], who employed the BKK gluon FF [10].

The comparisons presented in Fig. 10 provide us with a very useful check of the gluon FF in the low- x range, where the data have small errors. In particular, the good agreement in the case of flavour separation nicely confirms the relative importance of the light- and b -quark FFs relative to the gluon FF. Since the χ^2_{DF} values obtained at NLO for the longitudinal cross section are comparable to those achieved in our NLO fit, we do not expect that the inclusion of the information on the longitudinal cross section in our NLO fit would significantly change the outcome.

As is well known, the gluon FF only enters the prediction for $d\sigma^h/dx$ at $\mathcal{O}(\alpha_s)$, while at $\mathcal{O}(\alpha_s^0)$ it only contributes indirectly via the Q^2 evolution. Therefore, we have used the ALEPH [20] and OPAL [21] data on gluon-tagged three-jet events in order to constrain it. These data were already compared with the fitted gluon FF in Fig. 5. It is of interest to compare this gluon FF with the BKK [11] one and the one recently extracted by DELPHI [30] from their three-jet events for scales in the range $6.5 \leq M_f \leq 28$ GeV. In Ref. [30], a parameterization, valid for this M_f range and for $0.15 \leq x \leq 0.75$, was generated adopting an ansatz similar to the one introduced in Ref. [11]. In Fig. 11, the x dependences of these three gluon FFs are studied for $M_f = 10, 52.4, 80.2$, and 200 GeV. The results for $M_f = 52.4$ and 80.2 GeV are compared with the ALEPH [20] and OPAL [21] gluon-tagged three-jet data, which are included in our fits. From Fig. 11 the following observations can be made. Our new gluon FF is rather similar to the BKK one, especially for larger values of M_f . At $M_f = 80.2$ GeV, the DELPHI gluon FF is somewhat steeper than the new and BKK ones, except for large x values, and it agrees slightly better with the OPAL [21] data. On the other hand, our new gluon FF agrees best with the ALEPH [20] data at $M_f = 52.4$ GeV. At $M_f = 10$ GeV, the DELPHI gluon FF has a flatter x dependence than the other ones and overshoots them, while at $M_f = 200$ GeV the situation is similar to the case of $M_f = 80.2$ GeV.

4 Conclusions

The LEP1 and SLC experiments have provided us with a wealth of high-precision experimental information on how partons fragment into low-mass charged hadrons [2,13,14,15,16,17,18,19,20,21,23]. The data partly come as light-, c -, and b -quark-enriched samples without [14,15,23] or with identified final-state hadrons (π^\pm , K^\pm , and p/\bar{p}) [18,19] or as gluon-tagged three-jet samples without hadron identification [20,21,30]. This new situation motivated us to update, refine, and extend the BKK analysis [11] by generating new LO and NLO sets of π^\pm , K^\pm , and p/\bar{p} FFs. The x distributions of the resulting FFs at their starting scales Q_0 are given by Eq. (2) with the parameters listed in Table 2. The Q^2 evolution is determined by the timelike Altarelli-Parisi equations in the respective orders, LO or NLO, which are summarized in the Appendix of Ref. [38].¹ The evolution procedure in Mellin space is described in Ref. [11]. A FORTRAN subroutine which returns the values of the $D_a^h(x, Q^2)$ functions for given values of x and Q^2 may be downloaded from the URL <http://www.desy.de/~poetter/kkp.html> or obtained upon request from the authors.

By also including in our fits π^\pm , K^\pm , and p/\bar{p} data (without flavour separation) from PEP [12], with CM energy $\sqrt{s} = 29$ GeV, we obtained a handle on the scaling violation in the fragmentation process, which allowed us to extract LO and NLO values of $\alpha_s(M_Z)$. We found $\alpha_s(M_Z) = 0.1181^{+0.006}_{-0.007}$ at LO and $\alpha_s(M_Z) = 0.1170^{+0.005}_{-0.007}$ at NLO, where the errors are experimental. These results are in perfect agreement with what the Particle Data Group currently quotes as the world average, $\alpha_s(M_Z) = 0.1185 \pm 0.002$ [32].

Our strategy was to only include in our fits LEP1 and SLC data with both flavour separation and hadron identification [19,18], gluon-tagged three-jet samples with a fixed gluon-jet energy [20,21], and the π^\pm , K^\pm , and p/\bar{p} data sets from the pre-LEP1/SLC era with the highest statistics and the finest binning in x [12]. Other data served us for cross checks. In particular, we probed the scaling violation through comparisons with π^\pm , K^\pm , and p/\bar{p} data from DORIS and PETRA, with CM energies between 5.4 and 34 GeV [24,25,26,27]. Furthermore, we tested the gluon FF, which enters the unpolarized cross section only at NLO, by comparing our predictions for the longitudinal cross section, where it already enters at LO, with available data [14,28,29]. Finally, we directly compared our gluon FF with the one recently measured by DELPHI in three-jet production with gluon identification as a function of x at various scales Q^2 [30]. All these comparisons led to rather encouraging results. We also verified that our FFs satisfy reasonably well the momentum sum rules, which we did not impose as constraints on our fits. All these cross checks make us believe that our FFs should allow for a reliable description of inclusive charged-hadron production in all kinds of high-energy-collision experiments over wide ranges of x and Q^2 . The very-high- Q^2 regime will be accessible with the CERN LHC and a future e^+e^- linear collider. Our FFs are bound to break down at very low values of x , where it becomes necessary to modify the ansatz (2) according to the MLLA [36]. This is beyond the scope of the present analysis, but should eventually be investigated [35].

¹There is an obvious typographical error in the published version of Ref. [38], which was absent in the preprint version thereof. In the line before the last of Eq. (17), $\ln \ln(1-x)$ should be replaced by $\ln(1-x)$.

Note added

After the submission of this paper, a preprint [39] appeared which also presents NLO FFs for π^\pm , K^\pm , and charged hadrons. These FFs are fitted to the ALEPH [14,15], SLD [19], and TPC [12] data assuming certain power laws in the light-quark sector.

Acknowledgements

The II. Institut für Theoretische Physik is supported in part by the Deutsche Forschungsgemeinschaft through Grant No. KN 365/1-1, by the Bundesministerium für Bildung und Forschung through Grant No. 05 HT9GUA 3, and by the European Commission through the Research Training Network *Quantum Chromodynamics and the Deep Structure of Elementary Particles* under Contract No. ERBFMRX-CT98-0194.

References

- [1] P. Mättig, Phys. Rep. 177 (1989) 141.
- [2] ALEPH Collaboration, R. Barate et al., Phys. Rep. 294 (1998) 1.
- [3] G. Altarelli, R.K. Ellis, G. Martinelli, S.-Y. Pi, Nucl. Phys. B 160 (1979) 301; R. Baier, K. Fey, Z. Phys. C 2 (1979) 339.
- [4] P.J. Rijken, W.L. van Neerven, Phys. Lett. B 386 (1996) 422; B 392, 207 (1997); Nucl. Phys. B 487 (1997) 233; P.J. Rijken, PhD Thesis, Rijksuniversiteit te Leiden, March 1997.
- [5] R.D. Field, R.P. Feynman, Phys. Rev. D 15 (1977) 2590; Nucl. Phys. B 136 (1998) 1.
- [6] V. Barger, T. Gottschalk, R.J.N. Phillips, Phys. Lett. 70 B (1977) 51; J.F. Owens, E. Reya, M. Glück, Phys. Rev. D 18 (1978) 1501; R. Baier, J. Engels, B. Petersson, Z. Phys. C 2 (1979) 265; M. Anselmino, P. Kroll, E. Leader, Z. Phys. C 18 (1983) 307.
- [7] L.M. Sehgal, P.M. Zerwas, Nucl. Phys. B 108 (1976) 483; C. Peterson, D. Schlatter, I. Schmitt, P.M. Zerwas, Phys. Rev. D 27 (1983) 105.
- [8] P. Chiappetta, M. Greco, J.-Ph. Guillet, S. Rolli, M. Werlen, Nucl. Phys. B 412 (1994) 3.
- [9] M. Greco, S. Rolli, Z. Phys. C 60 (1993) 169; Phys. Rev. D 52 (1995) 3853; M. Greco, S. Rolli, A. Vicini, Z. Phys. C 65 (1995) 277.
- [10] J. Binnewies, B.A. Kniehl, G. Kramer, Z. Phys. C 65 (1995) 471.

- [11] J. Binnewies, B.A. Kniehl, G. Kramer, Phys. Rev. D 52 (1995) 4947.
- [12] TPC/Two-Gamma Collaboration, H. Aihara et al., LBL Report No. LBL-23737 and UC-34D, March 1988 (unpublished); Phys. Rev. Lett. 61 (1988) 1263.
- [13] G.D. Cowan, *in* Proceedings of the XXVII International Conference on High Energy Physics, Glasgow, Scotland, UK, 20–27 July 1994, edited by P.J. Bussey and I.G. Knowles (Institute of Physics Publishing, Bristol, 1995) p. 883.
- [14] ALEPH Collaboration, D. Buskulic et al., Phys. Lett. B 357 (1995) 487, B 364 (1995) 247 (E).
- [15] C. Padilla Aranda, PhD Thesis, Universitat Autònoma de Barcelona, September 1995.
- [16] ALEPH Collaboration, D. Buskulic et al., Z. Phys. C 66 (1995) 355.
- [17] OPAL Collaboration, P.D. Acton et al., Z. Phys. C 58 (1993) 387.
- [18] DELPHI Collaboration, P. Abreu et al., Eur. Phys. J. C 5 (1998) 585.
- [19] SLD Collaboration, K. Abe et al., Phys. Rev. D 59 (1999) 052001.
- [20] ALEPH Collaboration, R. Barate et al., Report No. CERN-EP/98-16, February 1998, submitted to Eur. Phys. J. C.
- [21] OPAL Collaboration, G. Abbiendi et al., Eur. Phys. J. C 11 (1999) 217.
- [22] J.W. Gary, Phys. Rev. D 49 (1994) 4503.
- [23] OPAL Collaboration, K. Ackerstaff et al., Eur. Phys. J. C 7 (1999) 369.
- [24] DASP Collaboration, R. Brandelik et al., Nucl. Phys. B 148 (1979) 189.
- [25] ARGUS Collaboration, H. Albrecht et al., Z. Phys. C 44 (1989) 547.
- [26] TASSO Collaboration, M. Althoff et al., Z. Phys. C 17 (1983) 5.
- [27] TASSO Collaboration, W. Braunschweig et al., Z. Phys. C 42 (1989) 189.
- [28] DELPHI Collaboration, P. Abreu et al., Eur. Phys. J. C 6 (1999) 19.
- [29] OPAL Collaboration, R. Akers et al., Z. Phys. C 68 (1995) 203.
- [30] DELPHI Collaboration, P. Abreu et al., Eur. Phys. J. C 13 (2000) 573.
- [31] F. James, M. Roos, Comput. Phys. Commun. 10 (1975) 343.

- [32] Particle Data Group, C. Caso et al., Eur. Phys. J. C 3 (1998) 1 and 1999 off-year partial update for the 2000 edition available on the PDG WWW pages (URL: <http://pdg.lbl.gov/>).
- [33] DELPHI Collaboration, W. Adam et al., Z. Phys. C 69 (1996) 561.
- [34] ARGUS Collaboration, H. Albrecht et al., Z. Phys. C 44 (1989) 547;
TASSO Collaboration, W. Braunschweig et al., Z. Phys. C 47 (1990) 167;
ALEPH Collaboration, D. Buskulic et al., Z. Phys. C 64 (1994) 361;
OPAL Collaboration, R. Akers et al., Z. Phys. C 67 (1995) 389.
- [35] B.A. Kniehl, G. Kramer, W. Ochs, B. Pötter, in preparation.
- [36] For a review, see V.A. Khoze, W. Ochs, Int. J. Mod. Phys. A 12 (1997) 2949.
- [37] J. Binnewies, PhD Thesis, Universität Hamburg, Report No. DESY 97-128 and hep-ph/9707269, July 1997.
- [38] J. Binnewies, B.A. Kniehl, G. Kramer, Z. Phys. C 76 (1997) 677.
- [39] S. Kretzer, Phys. Rev. D 62 (2000) 054001.

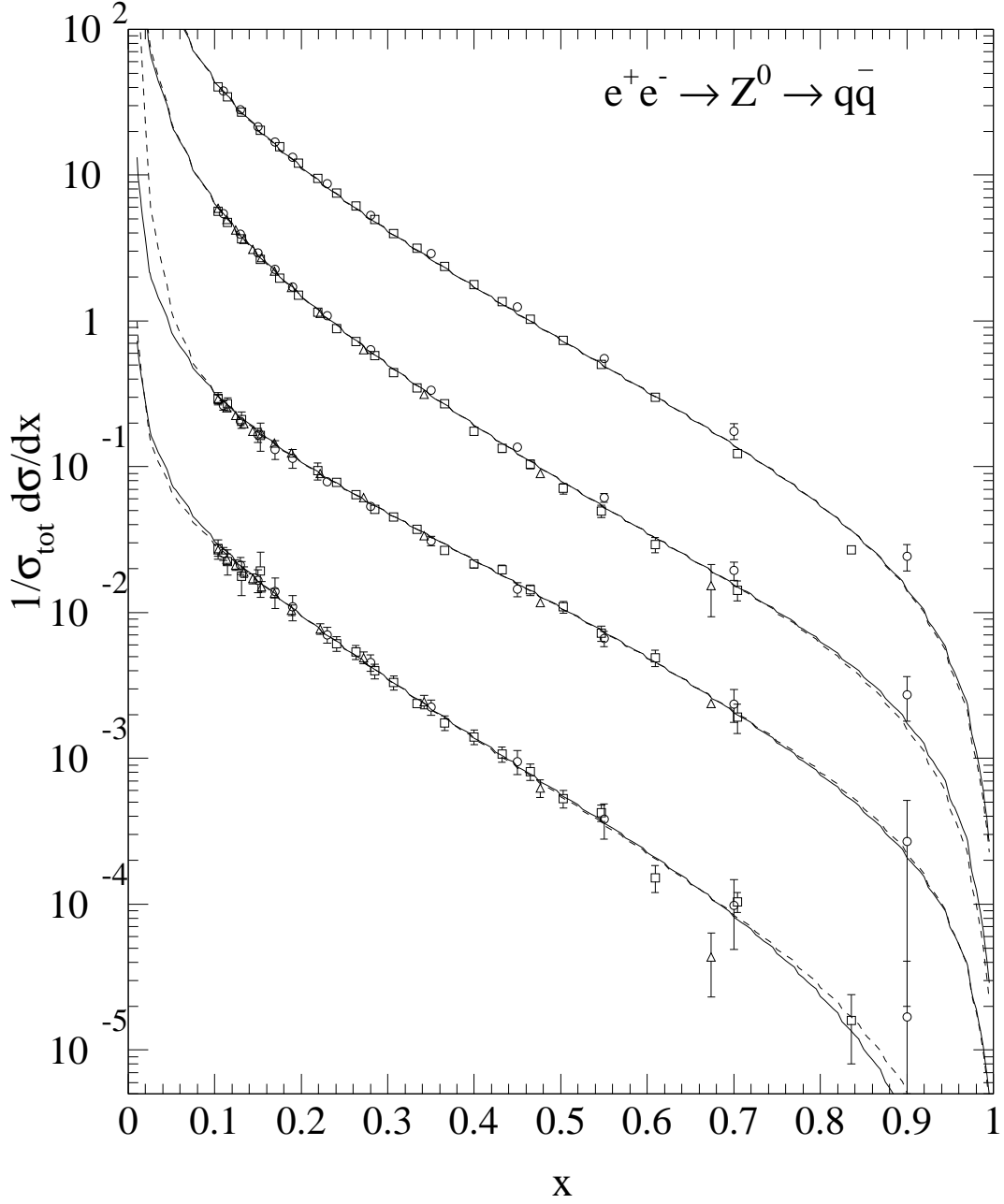


Figure 1: Normalized differential cross section of inclusive hadron production at $\sqrt{s} = 91.2$ GeV as a function of x . The LO (dashed lines) and NLO (solid lines) fit results are compared with data from ALEPH [16] (triangles), DELPHI [18] (circles), and SLD [19] (squares). The upmost, second, third, and lowest curves refer to charged hadrons, π^\pm , K^\pm , and p/\bar{p} , respectively. Each pair of curves is rescaled relative to the nearest upper one by a factor of $1/5$.

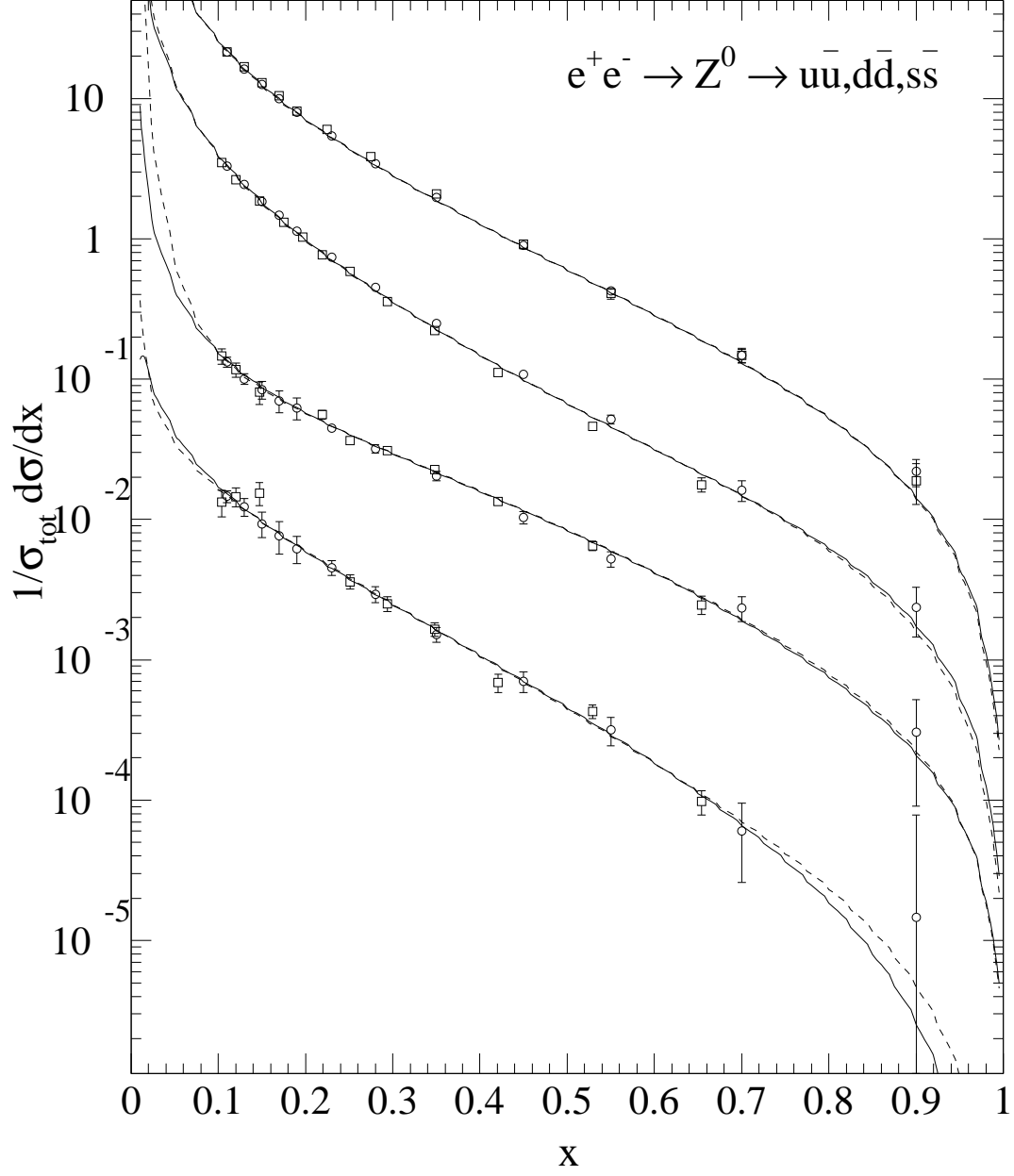


Figure 2: Same as in Fig. 1, but for the light-quark-enriched samples from DELPHI [18] (circles) and SLD [19] (squares).

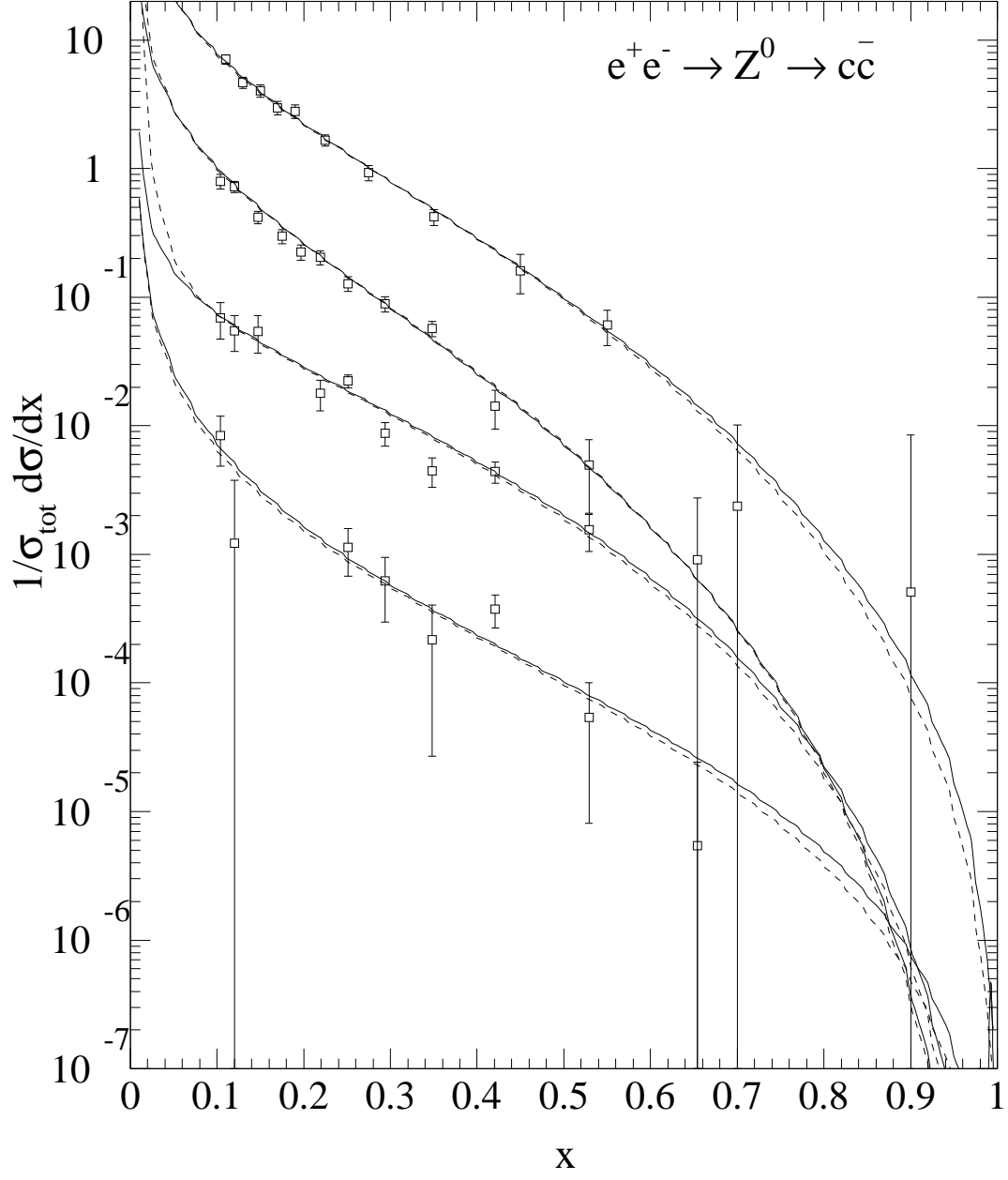


Figure 3: Same as in Fig. 1, but for the c -quark-enriched samples from SLD [19] (squares). The last two points on the right belong to the charged-hadron sample.

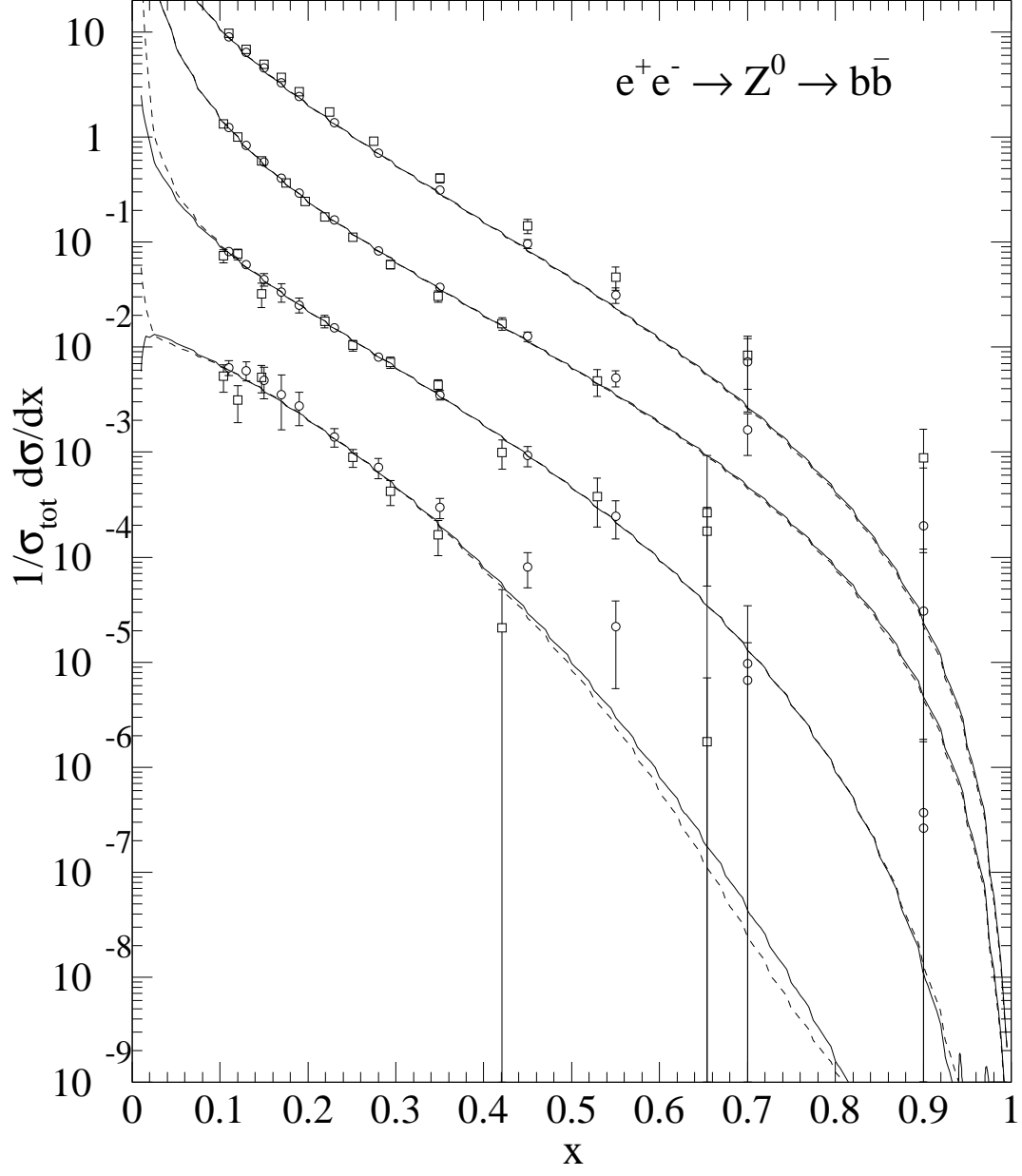


Figure 4: Same as in Fig. 1, but for the b -quark-enriched samples from DELPHI [18] (circles) and SLD [19] (squares).

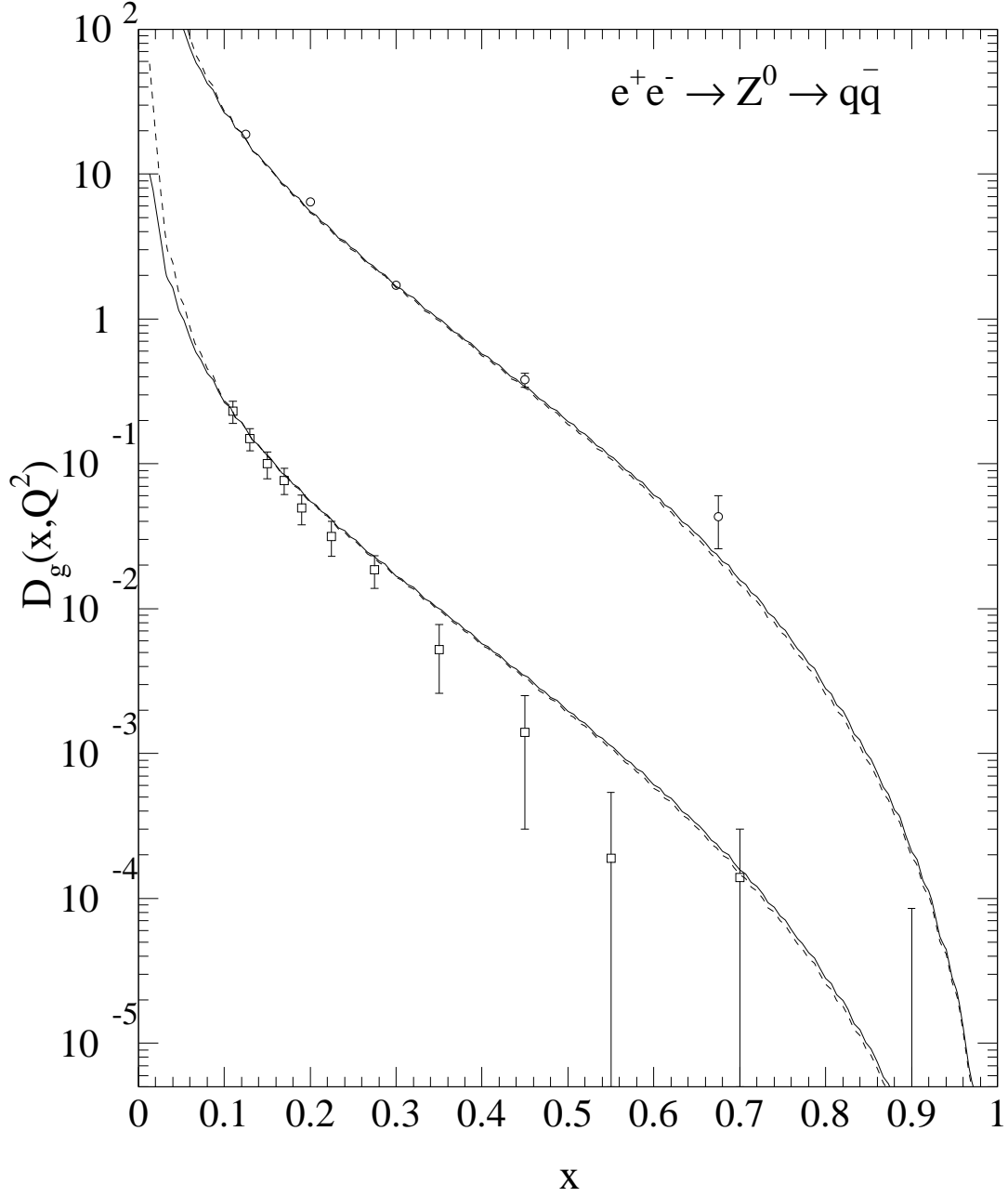


Figure 5: Gluon FF for charged-hadron production as a function of x at $M_f = 52.4$ and 80.2 GeV. The LO (dashed lines) and NLO (solid lines) predictions are compared with three-jet data from ALEPH [20], with $E_{\text{jet}} = 26.2$ GeV, (upper curves) and from OPAL [21], with $E_{\text{jet}} = 40.1$ GeV (lower curves). The OPAL data and the pertinent predictions are rescaled by a factor of $1/100$.

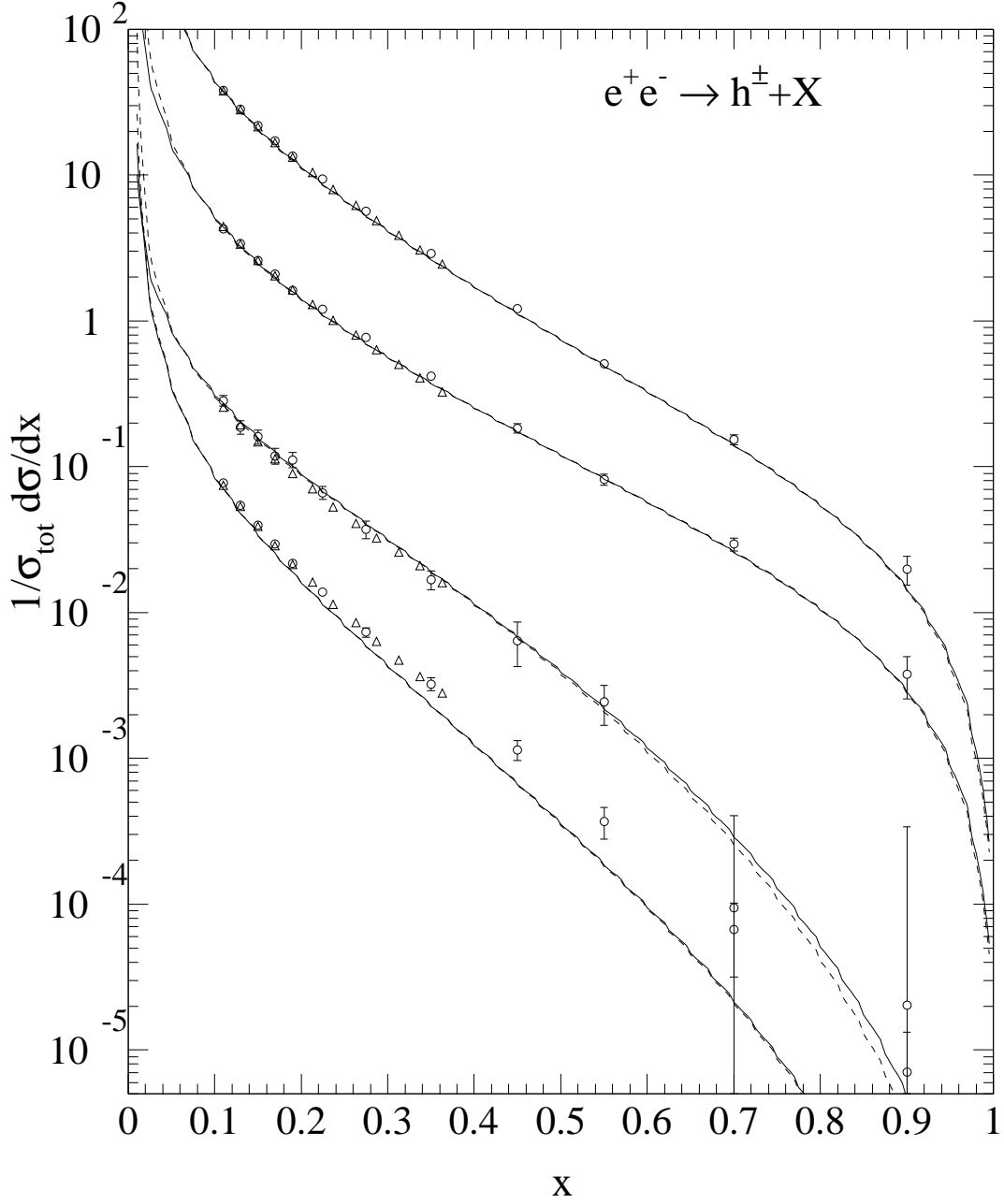


Figure 6: Normalized differential cross section of inclusive charged-hadron production at $\sqrt{s} = 91.2$ GeV as a function of x . The LO (dashed lines) and NLO (solid lines) fit results are compared with data from ALEPH [14,15] (triangles) and OPAL [23] (circles). The upmost, second, third, and lowest curves refer to the full, light-quark-enriched, c -quark-enriched, and b -quark-enriched samples, respectively. Each pair of curves is rescaled relative to the nearest upper one by a factor of $1/5$.

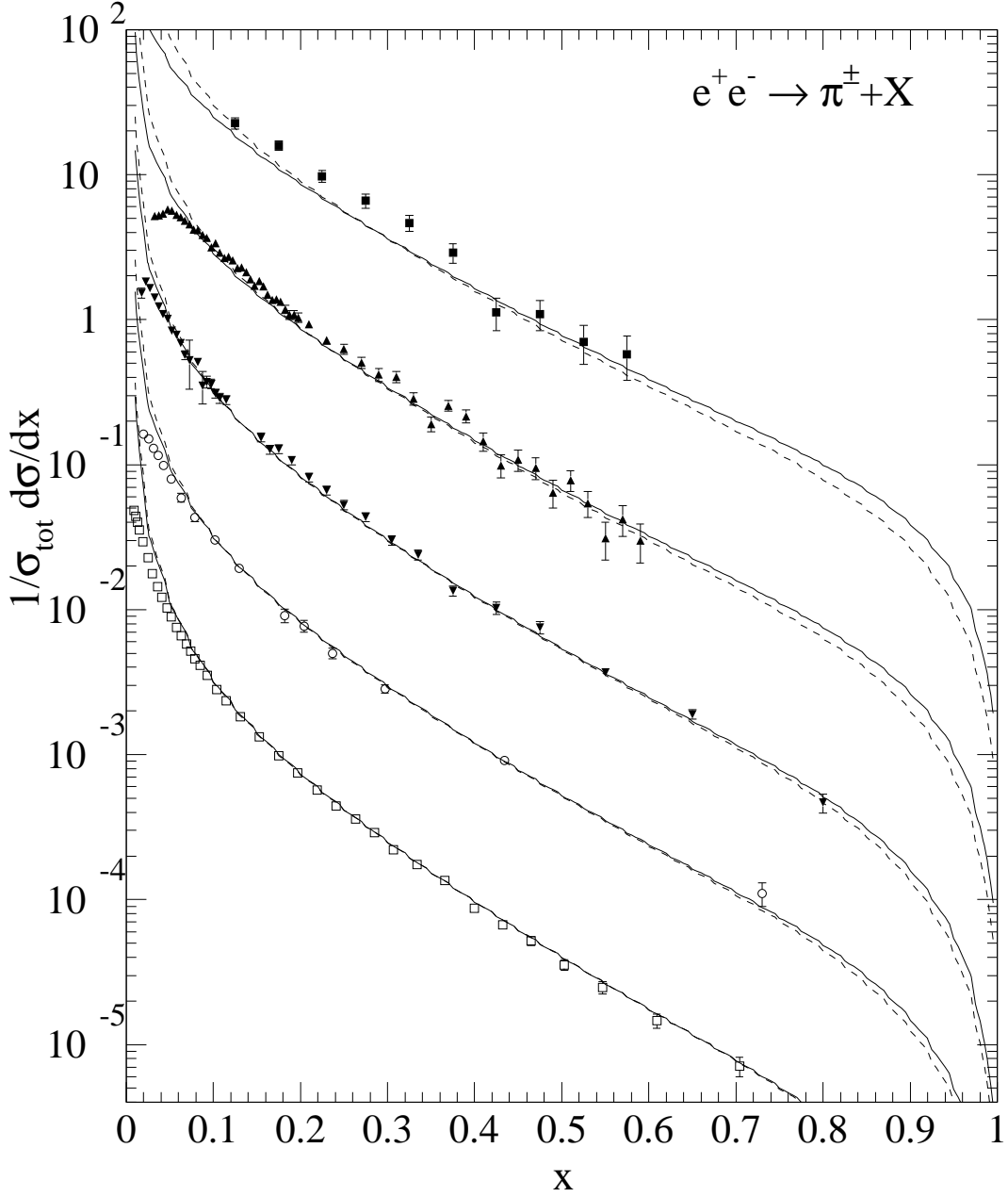


Figure 7: Normalized differential cross section of inclusive π^\pm production as a function of x at $\sqrt{s} = 5.2, 9.98, 29, 34,$ and 91.2 GeV. The LO (dashed lines) and NLO (solid lines) predictions are compared with data from DASP [24], ARGUS [25], TPC [12], TASSO [27], and SLD [19]. Upper curves correspond to lower energies. Each pair of curves is rescaled relative to the nearest upper one by a factor of $1/10$.

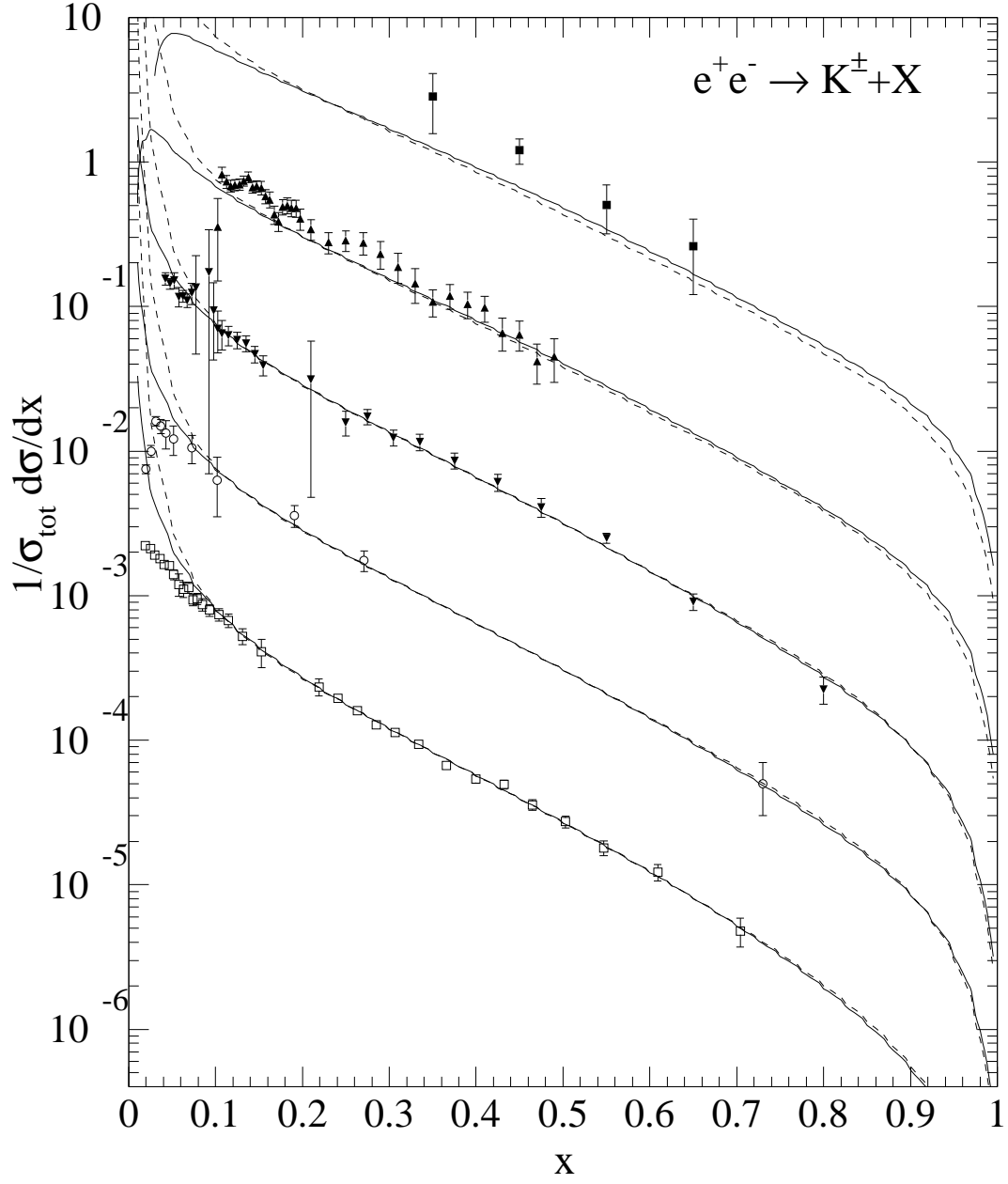


Figure 8: Same as in Fig. 7, but for K^\pm mesons.

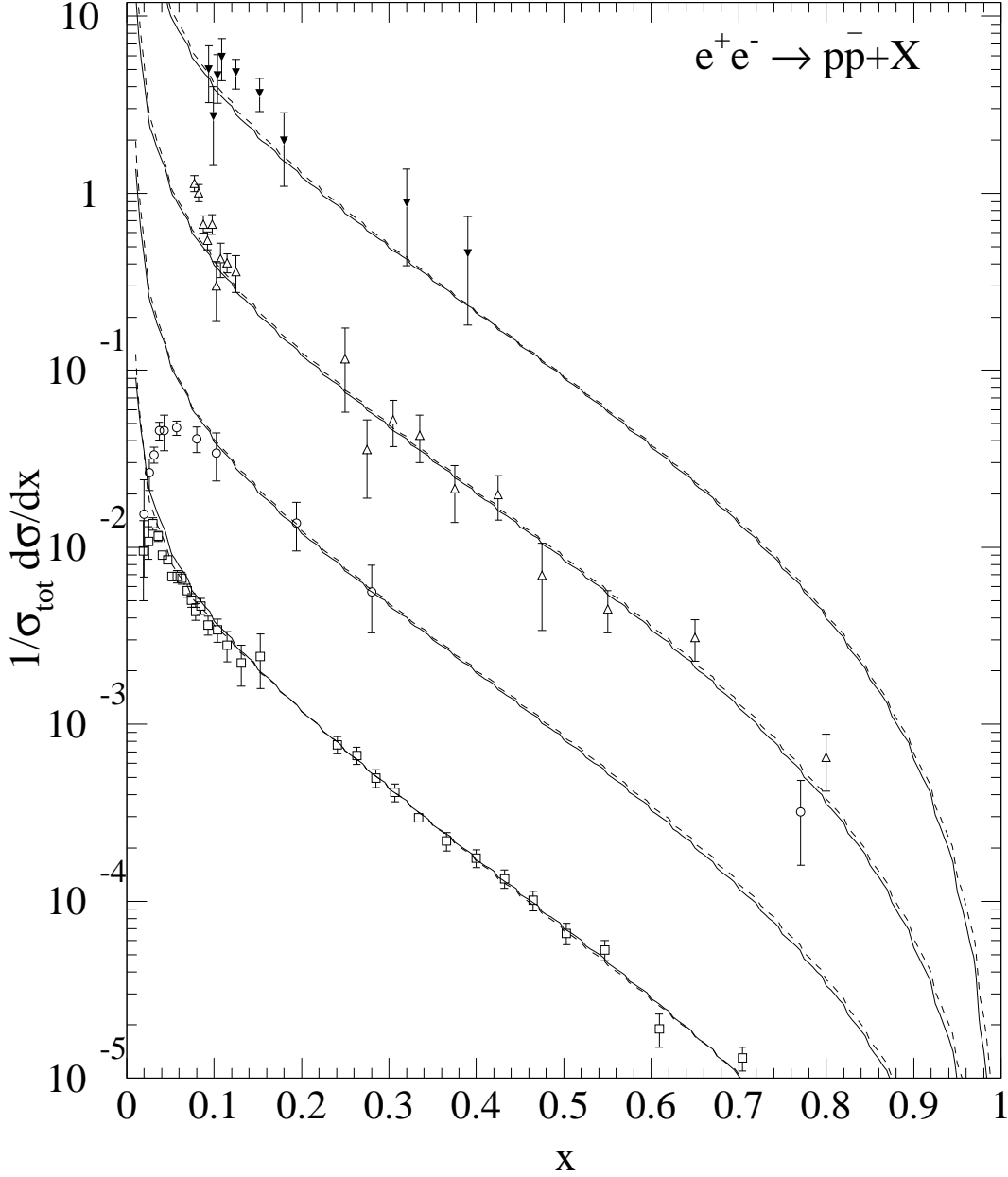


Figure 9: Normalized differential cross section of inclusive p/\bar{p} production as a function of x at $\sqrt{s} = 22, 29, 34$, and 91.2 GeV. The LO (dashed lines) and NLO (solid lines) predictions are compared with data from TASSO (with $\sqrt{s} = 22$ [26] and 34 GeV [27]), TPC [12], and SLD [19]. Upper curves correspond to lower energies. Each pair of curves is rescaled relative to the nearest upper one by a factor of $1/10$.

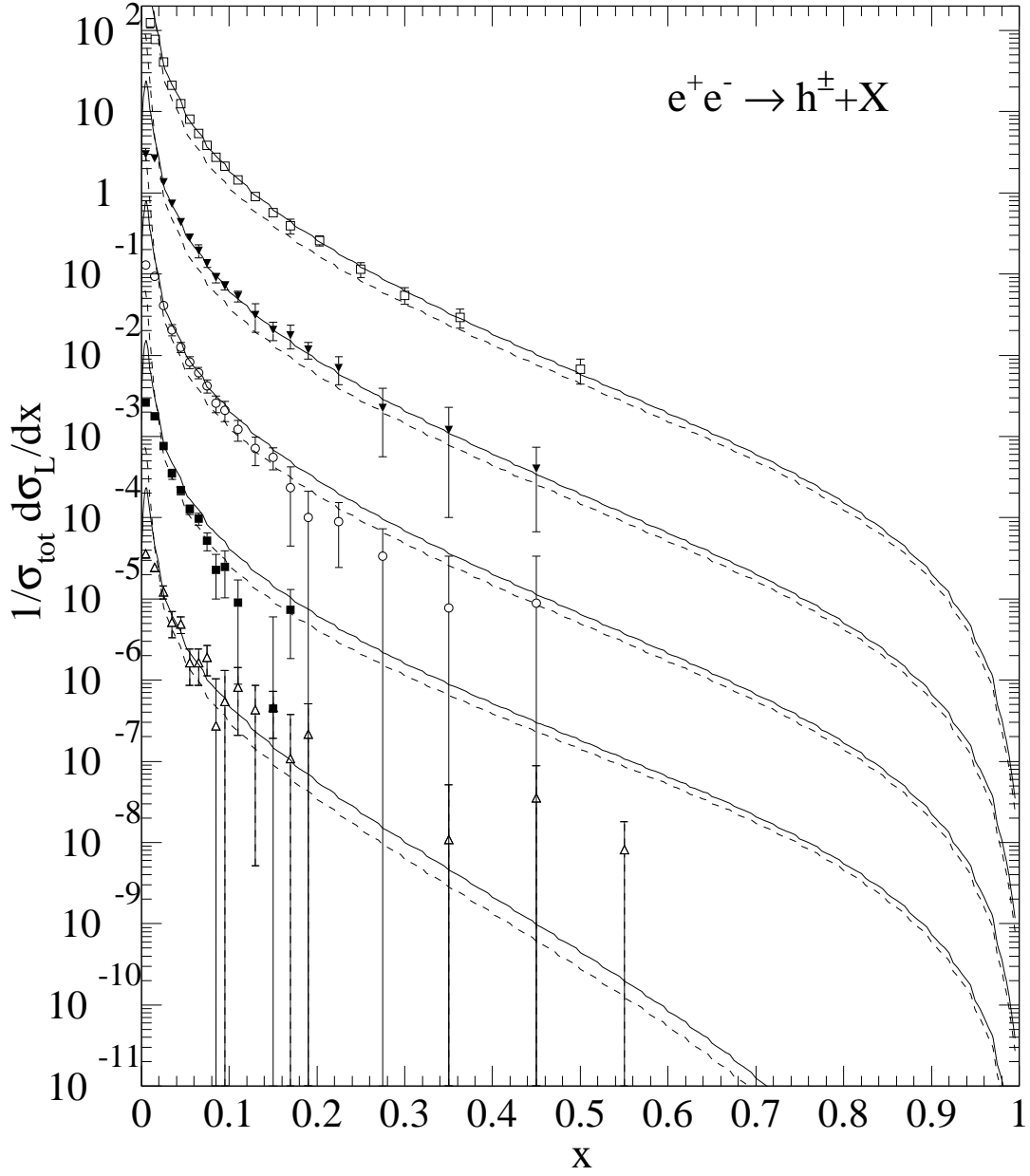


Figure 10: Normalized differential longitudinal cross section of inclusive charged-hadron production as a function of x at $\sqrt{s} = 91.2$ GeV. The LO (dashed lines) and NLO (solid lines) predictions are compared with data from ALEPH [14], OPAL [29], and DELPHI [28] without flavour separation and with light- and b -quark-enriched samples from DELPHI [28] (in this order from top to bottom). Each pair of curves is rescaled relative to the nearest upper one by a factor of $1/30$.

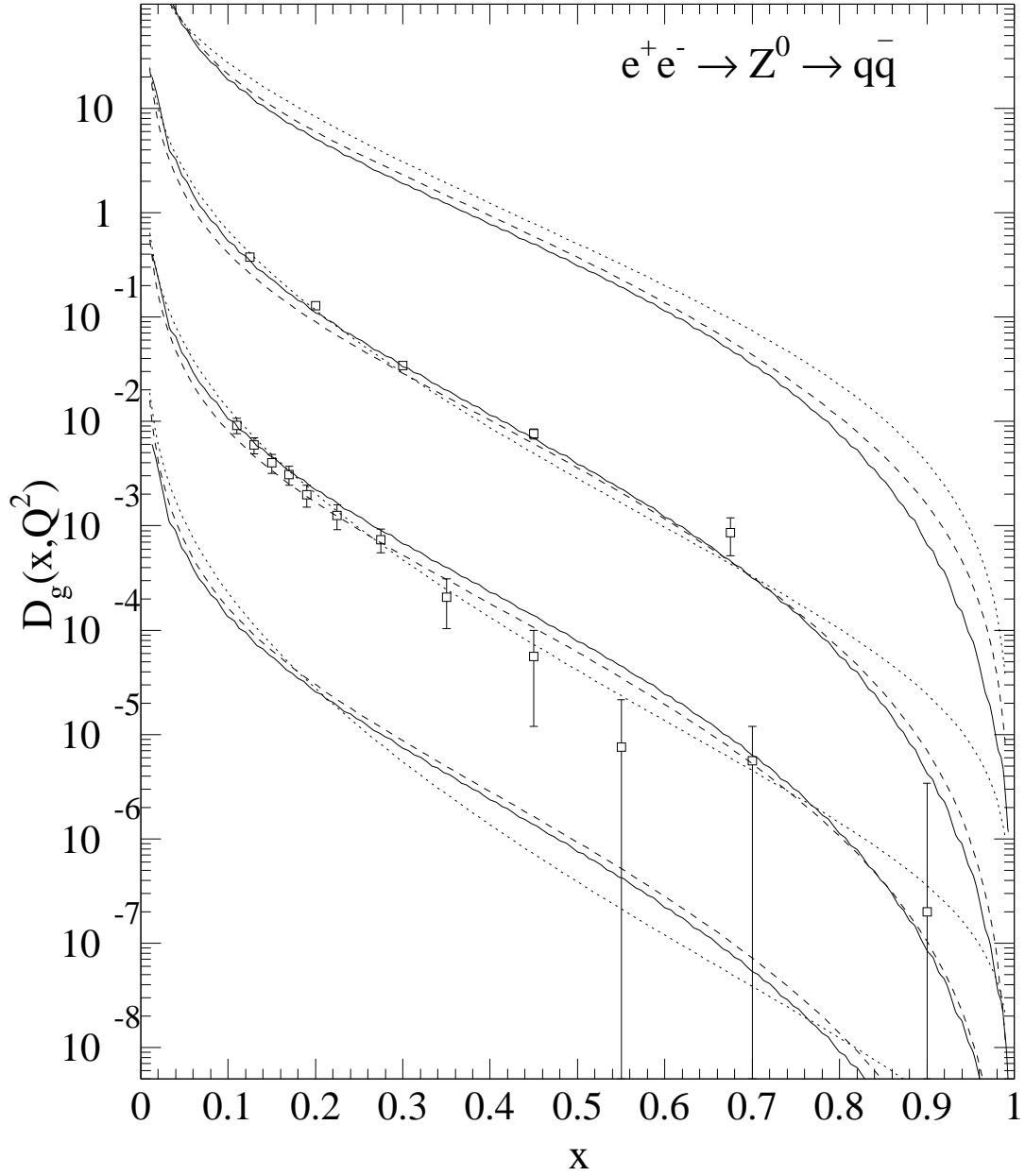


Figure 11: Gluon FFs for charged-hadron production as functions of x at $M_f = 10, 52.4, 80.2,$ and 200 GeV from the DELPHI [21] (dotted lines), BKK NLO [11] (dashed lines), and new NLO (solid lines) sets. The predictions for $M_f = 52.4$ and 80.2 GeV are compared with the gluon-tagged three-jet data from ALEPH [20] and OPAL [21], respectively. Upper curves correspond to lower energies. Each set of curves is rescaled relative to the nearest upper one by a factor of $1/50$.